
Partial success in closing the gap between human and machine vision

Robert Geirhos^{1-2§}

Kanharaju Narayanappa¹

Benjamin Mitzkus¹

Tizian Thieringer¹

Matthias Bethge^{1*}

Felix A. Wichmann^{1*}

Wieland Brendel^{1*}

¹University of Tübingen

²International Max Planck Research School for Intelligent Systems

*Joint senior authors

§To whom correspondence should be addressed: robert.geirhos@uni-tuebingen.de

Abstract

A few years ago, the first CNN surpassed human performance on ImageNet. However, it soon became clear that machines lack robustness on more challenging test cases, a major obstacle towards deploying machines “in the wild” and towards obtaining better computational models of human visual perception. Here we ask: Are we making progress in closing the gap between human and machine vision? To answer this question, we tested human observers on a broad range of out-of-distribution (OOD) datasets, adding the “missing human baseline” by recording 85,120 psychophysical trials across 90 participants. We then investigated a range of promising machine learning developments that crucially deviate from standard supervised CNNs along three axes: objective function (self-supervised, adversarially trained, CLIP language-image training), architecture (e.g. vision transformers), and dataset size (ranging from 1M to 1B).

Our findings are threefold. (1.) The longstanding *robustness gap* between humans and CNNs is closing, with the best models now matching or exceeding human performance on most OOD datasets. (2.) There is still a substantial image-level *consistency gap*, meaning that humans make different errors than models. In contrast, most models systematically agree in their categorisation errors, even substantially different ones like contrastive self-supervised vs. standard supervised models. (3.) In many cases, human-to-model consistency improves when training dataset size is increased by one to three orders of magnitude. Our results give reason for cautious optimism: While there is still much room for improvement, the behavioural difference between human and machine vision is narrowing. In order to measure future progress, 17 OOD datasets with image-level human behavioural data are provided as a benchmark at <https://github.com/bethgelab/model-vs-human/>.

1 Introduction

Looking back at the last decade, deep learning has made tremendous leaps of progress by any standard. What started in 2012 with AlexNet [1] as the surprise winner of the ImageNet Large-Scale Visual Recognition Challenge quickly became the birth of a new AI “summer”, a summer lasting much longer than just a season. With it, just like with any summer, came great expectations: the hope that the deep learning revolution will see widespread applications in industry, that it will propel breakthroughs in the sciences, and that it will ultimately close the gap between human and machine perception.

We have now reached the point where deep learning has indeed become a significant driver of progress in industry [e.g. 2, 3], and where many disciplines are employing deep learning for scientific discoveries [4–9]—*but are we making progress in closing the gap between human and machine vision?*

For a long time, the gap between human and machine vision was mainly approximated by comparing benchmark accuracies on IID (independent and identically distributed) test data: as long as models are far from reaching human-level performance on challenging datasets like ImageNet, this approach is adequate [10]. Currently, models are routinely matching and in many cases even outperforming humans on IID data. At the same time, it is becoming increasingly clear that models systematically exploit shortcuts shared between training and test data [11–14]. Therefore we are witnessing a major shift towards measuring model performance on out-of-distribution (OOD) data rather than IID data alone, which aims at testing models on more challenging test cases where there is still a ground truth category, but certain image statistics differ from the training distribution. Many OOD generalisation datasets have been proposed, such as ImageNet-C [15] for corruption robustness, ImageNet-Sketch [16] for robustness towards sketches, and Stylized-ImageNet [17] for robustness towards image style changes. What most of these datasets have in common, however, is that they lack human comparison data. This is unfortunate, since we can no longer assume that humans reach near-ceiling accuracies on these challenging test cases as they do on standard noise-free IID object recognition datasets. In order to address this issue, we carefully tested human observers in a psychophysics laboratory on a broad range of OOD datasets, adding the “missing human baseline” by providing some 85K psychophysical trials across 90 participants. Crucially, we showed exactly the same images to multiple observers, which means that we are able to compare human and machine vision on the fine-grained level of individual images [18–20]).

The resulting 17 OOD datasets with large-scale human comparison data enable us to investigate recent exciting machine learning developments that crucially deviate from “vanilla” CNNs along three axes: objective function (supervised vs. self-supervised, adversarially trained, and CLIP’s joint language-image training), architecture (convolutional vs. vision transformer) and training dataset size (ranging from 1M to 1B images). Taken together, these are some of the most promising directions our field has developed to date—but this field would not be machine learning if new breakthroughs weren’t within reach in the next few weeks, months and years. Therefore, we will open-source `modelvshuman`, a Python project that enables testing both PyTorch and TensorFlow models on our comprehensive benchmark suite of OOD generalisation data in order to measure future progress. Even today, our results give cause for (cautious) optimism. After a method overview (Section 2), we are able to report that the human-machine *robustness gap* is closing: the best models now match or exceed human performance on most OOD datasets (Section 3). While there is still a substantial image-level *consistency gap* between humans and machines, this gap is narrowing on some—but not all—datasets when the size of the training dataset is increased (Section 4).

2 Methods: datasets, psychophysical experiments, models, metrics, toolbox

OOD datasets with consistency-grade human data. We collected human data for 17 generalisation datasets (visualized in Figures 7 and 8 in the Appendix) on a carefully calibrated screen in a dedicated psychophysical laboratory (a total of 85,120 trials across 90 observers). Five datasets each correspond to a single manipulation (sketches, edge-filtered images, silhouettes, images with a texture-shape cue conflict, and stylized images where the original image texture is replaced by the style of a painting); the remaining twelve datasets correspond to parametric image degradations (e.g. different levels of noise or blur). Those OOD datasets have in common that they are designed to test ImageNet-trained models. OOD images were obtained from different sources: sketches from ImageNet-Sketch [16], stylized images from Stylized-ImageNet [17], edge-filtered images, silhouettes and cue conflict images from [17]¹, and the remaining twelve parametric datasets were adapted from [21]. For these parametric datasets, [21] collected human accuracies but unfortunately, they showed different images to different observers implying that we cannot use their human data to assess image-level consistency between humans and machines. Thus we collected psychophysical data for those images ourselves by showing exactly the same images to multiple observers for each of those twelve datasets.

¹For those three datasets consisting of 160, 160 and 1280 images respectively, consistency-grade psychophysical data was already collected by the authors and included in our benchmark with permission from the authors.

Additionally, we cropped the images from [21] to 224×224 pixels to allow for a fair comparison to ImageNet models (all models included in our comparison receive 224×224 input images; [21] showed 256×256 images to human observers in many cases).

Psychophysical experiments. 90 observers were tested in a darkened chamber. Stimuli were presented at the center of a 22" monitor with 1920×1200 pixels resolution (refresh rate: 120 Hz). Viewing distance was 107 cm and target images subtended 3×3 degrees of visual angle. Human observers were presented with an image and asked to select the correct category out of 16 basic categories (such as chair, dog, airplane, etc.). Stimuli were balanced w.r.t. classes and presented in random order. For ImageNet-trained models, in order to obtain a choice from the same 16 categories, the 1,000 class decision vector was mapped to those 16 classes using the WordNet hierarchy [22].² We closely followed the experimental protocol defined by [21], who presented images for 200 ms followed by a $1/f$ backward mask to limit the influence of recurrent processing (otherwise comparing to feedforward models would be difficult). Further experimental details are provided in Appendix C.

Models. In order to disentangle the influence of objective function, architecture and training dataset size, we tested a total of 52 models: 24 standard ImageNet-trained CNNs [23], 8 self-supervised models [24–29],³ 6 Big Transfer models [31], 5 adversarially trained models [32], 5 vision transformers [33, 34], two semi-weakly supervised models [35] as well as Noisy Student [36] and CLIP [37]. Technical details for all models are provided in the Appendix.

Metrics. In addition to *OOD accuracy* (averaged across conditions and datasets), the following three metrics quantify how closely machines are aligned with the decision behaviour of humans.

Accuracy difference $A(m)$ is a simple aggregate measure that compares the accuracy of a machine m to the accuracy of human observers in different out-of-distribution tests,

$$A(m) : \mathbb{R} \rightarrow [0, 1], m \mapsto \frac{1}{|D|} \sum_{d \in D} \frac{1}{|H_d|} \sum_{h \in H_d} \frac{1}{|C_d|} \sum_{c \in C_d} (\text{acc}_{d,c}(h) - \text{acc}_{d,c}(m))^2 \quad (1)$$

where $\text{acc}_{d,c}(\cdot)$ is the accuracy of the model or the human on dataset $d \in D$ and condition $c \in C_d$ (e.g. a particular noise level), and $h \in H_D$ denotes a human observer tested on dataset d . Analogously, one can compute the average accuracy difference between a human observer h_1 and all other human observers by substituting h_1 for m and $h \in H_D \setminus \{h_1\}$ for $h \in H_D$ (which can also be applied for the two metrics defined below).

Aggregated metrics like $A(m)$ ignore individual image-level decisions. Two models with vastly different image-level decision behaviour might still end up with the same accuracies on each dataset and condition. Hence, we include two additional metrics in our benchmark that are sensitive to decisions on individual images.

Observed consistency $O(m)$ [20] measures the fraction of samples for which humans and a model m get the same sample either both right or both wrong. More precisely, let $b_{h,m}(s)$ be one if both a human observer h and m decide either correctly or incorrectly on a given sample s , and zero otherwise. We calculate the average observed consistency as

$$O(m) : \mathbb{R} \rightarrow [0, 1], m \mapsto \frac{1}{|D|} \sum_{d \in D} \frac{1}{|H_d|} \sum_{h \in H_d} \frac{1}{|C_d|} \sum_{c \in C_d} \frac{1}{|S_{d,c}|} \sum_{s \in S_{d,c}} b_{h,m}(s) \quad (2)$$

where $s \in S_{d,c}$ denotes a sample s (in our case, an image) of condition c from dataset d . Note that this measure can only be zero if the accuracy of h and m are exactly the same in each dataset and condition.

Error consistency $E(m)$ [20] tracks whether there is above-chance consistency. This is an important distinction, since e.g. two decision makers with 95% accuracy each will have at least 90% observed consistency, even if their 5% errors occur on non-overlapping subsets of the test data (intuitively, they both get most images correct and thus observed overlap is high). To this end, error consistency (a.k.a. Cohen’s kappa, cf. [38]) indicates whether the observed consistency is larger than what could have

²The appendix of [21] describes in more detail how this mapping is optimal using the ‘average’ probability aggregation method (“Aggregating probabilities from coarse classes”).

³We presented a preliminary and much less comprehensive version of this work at a NeurIPS workshop: Geirhos et al. [30].

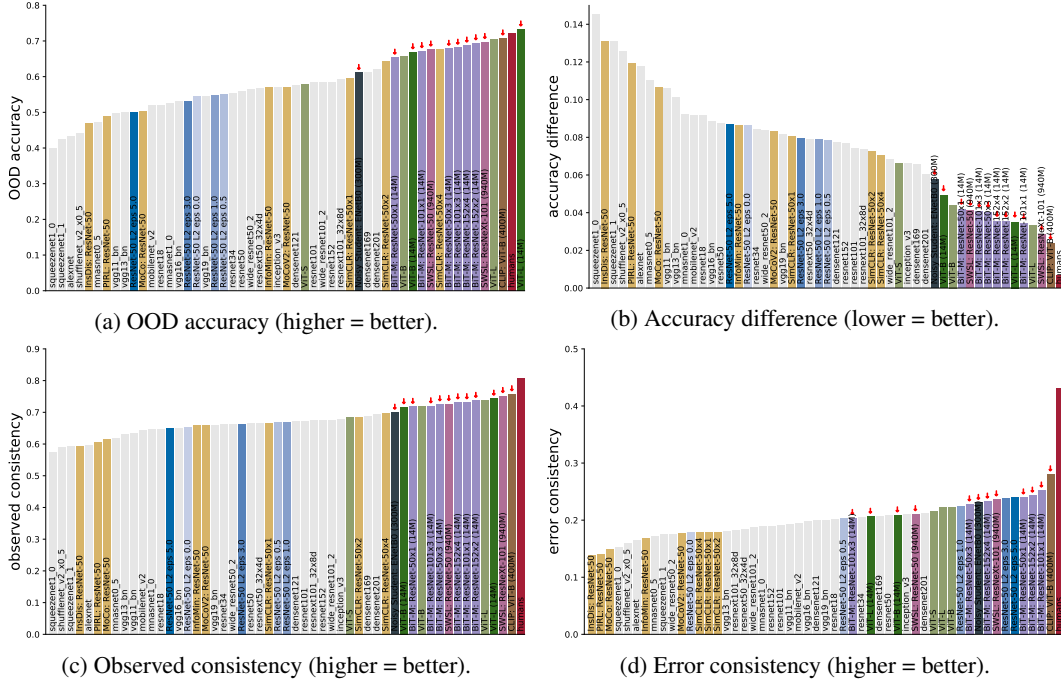


Figure 1: Core results, aggregated over 17 out-of-distribution (OOD) datasets: The OOD robustness gap between human and machine vision is closing (top), but an image-level consistency gap remains (bottom). Results compare humans, standard supervised CNNs, self-supervised models, adversarially trained models, vision transformers, noisy student, BiT, SWSL and CLIP. For convenience, ↓ marks models that are trained on large-scale datasets. Metrics defined in Section 2. Best viewed on screen.

been expected given two independent binomial decision makers with matched accuracy, which we denote as $\hat{o}_{h,m}$. This can easily be computed analytically [e.g. 20, equation 1]. Then, the average error consistency is given by

$$E(m) : \mathbb{R} \rightarrow [-1, 1], m \mapsto \frac{1}{|D|} \sum_{d \in D} \frac{1}{|H_d|} \sum_{h \in H_d} \frac{1}{|C_d|} \sum_{c \in C_d} \frac{(\frac{1}{|S_{d,c}|} \sum_{s \in S_{d,c}} b_{h,m}(s)) - \hat{o}_{h,m}(S_{d,c})}{1 - \hat{o}_{h,m}(S_{d,c})} \quad (3)$$

Benchmark & toolbox. $A(m)$, $O(m)$ and $E(m)$ each quantify a certain aspect of the human-machine gap. We use the mean rank order across these metrics to determine an overall model ranking (Table 2 in the Appendix). However, we would like to emphasise that the primary purpose of this benchmark is to generate insights, not winners. Since insights are best gained from detailed plots and analyses, we open-source `modelvshuman`, a Python project to benchmark models against human data.⁴ The current model zoo already includes 50+ models, and an option to add new ones (both PyTorch and TensorFlow). Evaluating a model will produce a 15+ page report on model behaviour. All plots in this paper can be generated for future models—to track whether they narrow the gap towards human vision, or to determine whether an algorithmic modification to a baseline model (e.g., an architectural improvement) changes model behaviour.

3 Robustness across models: the OOD robustness gap between human and machine vision is closing

We are interested in measuring whether we are making progress in closing the gap between human and machine vision. For a long time, CNNs were unable to match human robustness in terms of generalisation beyond the training distribution—a large OOD *robustness gap* [14, 21, 39, 40]. Having

⁴Of course, comparing human and machine vision is not limited to object recognition behaviour: other comparisons may be just as valid and interesting.

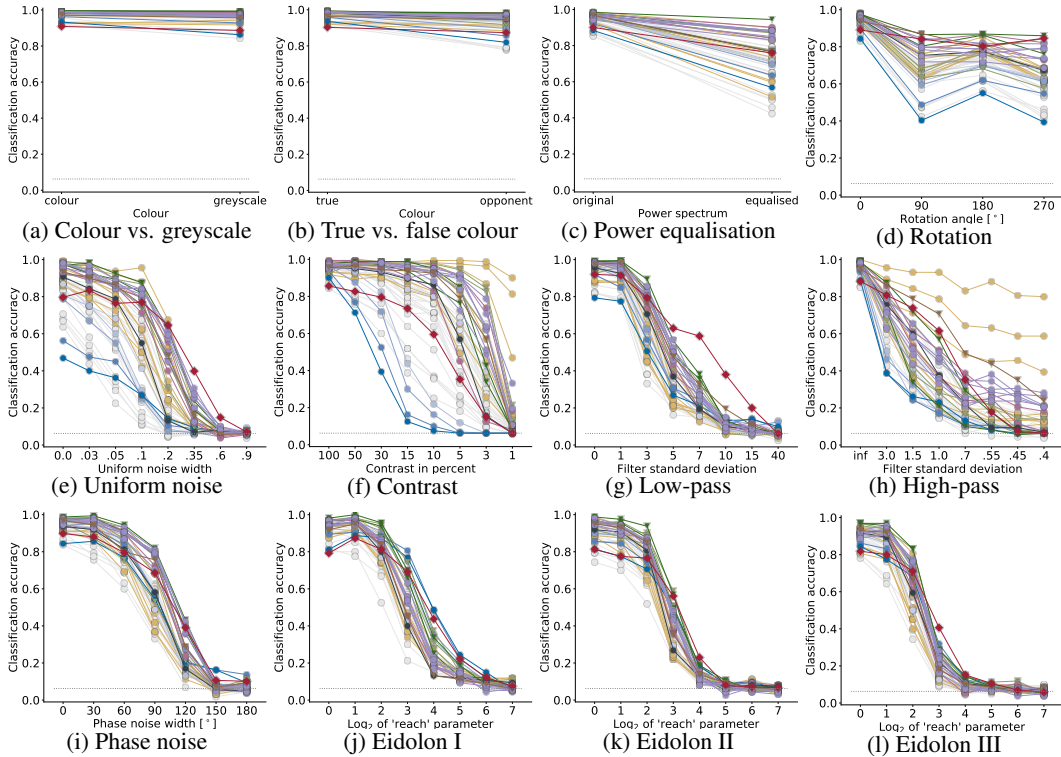


Figure 2: The OOD robustness gap between human and machine vision is closing. Robustness towards parametric distortions for **humans**, standard supervised CNNs, **self-supervised models**, adversarially trained models, vision transformers, noisy student, BiT, SWSL, CLIP. Symbols indicate architecture type (\circ convolutional, ∇ vision transformer, \diamond human); best viewed on screen.

tested human observers on 17 OOD datasets, we are now able to compare the latest developments in machine vision to human perception. Our core results are shown in Figure 1: the OOD robustness gap between human and machine vision is closing (1a, 1b), especially for models trained on large-scale datasets. On the individual image level, a human-machine consistency gap remains (especially 1d), which will be discussed later.

Self-supervised models “If intelligence is a cake, the bulk of the cake is unsupervised learning, the icing on the cake is supervised learning and the cherry on the cake is reinforcement learning”, Yann LeCun said in 2016 [41]. A few years later, the entire cake is finally on the table—the representations learned via self-supervised learning⁵ now compete with supervised methods on ImageNet [29] and outperform supervised pre-training for object detection [27]. But how do recent self-supervised models differ from their supervised counterparts in terms of their behaviour? Do they bring machine vision closer to human vision? Humans, too, rapidly learn to recognise new objects without requiring hundreds of labels per instance; additionally a number of studies reported increased similarities between self-supervised models and human perception [42–46]. Figure 2 compares the generalisation behaviour of eight self-supervised models in orange (PIRL, MoCo, MoCoV2, InfoMin, InsDis, SimCLR-x1, SimCLR-x2, SimCLR-x4)—with 24 standard supervised models (grey). We find only marginal differences between self-supervised and supervised models: Across distortion types, self-supervised networks are well within the range of their poorly generalising supervised counterparts. However, there is one exception: the three SimCLR variants show strong generalisation improvements on uniform noise, low contrast, and high-pass images, where they are the three top-performing self-supervised networks—quite remarkable given that SimCLR models were trained on a different set of augmentations (random crop with flip and resize, colour distortion, and Gaussian blur). Curious by the outstanding performance of SimCLR, we asked whether the self-supervised objective

⁵“Unsupervised learning” and “self-supervised learning” are sometimes used interchangeably. We use the term “self-supervised learning” since those methods use (label-free) supervision.

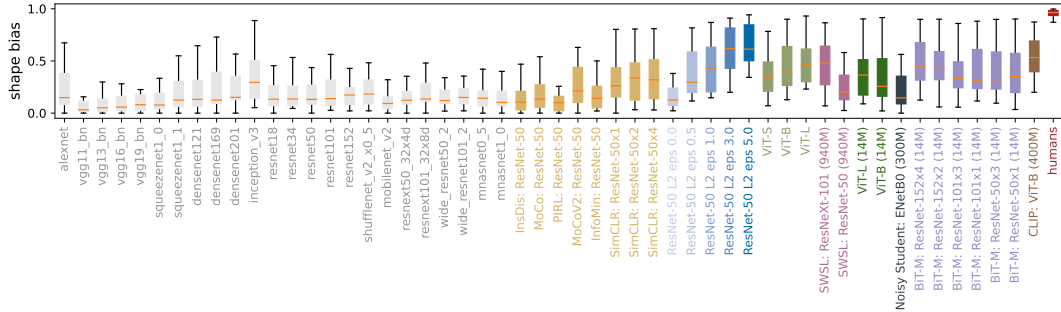


Figure 3: Shape (top) vs. texture (bottom) biases of different models. While human shape bias is not yet matched, several approaches improve over vanilla CNNs. Box plots show category-dependent distribution of shape/texture biases.

function or the choice of training data augmentations was the defining factor. When comparing self-supervised SimCLR models with augmentation-matched baseline models trained in the standard supervised fashion (Figure 15 in the Appendix), we find that the augmentation scheme (rather than the self-supervised objective) indeed made the crucial difference: supervised baselines show just the same generalisation behaviour, a finding that fits well with [47], who observed that the influence of training data augmentations is stronger than the role of architecture or training objective. In conclusion, our analyses indicate that the “cake” of contrastive self-supervised learning currently (and disappointingly) tastes much like the “icing”.

Adversarially trained models The vulnerability of CNNs to adversarial input perturbations is, arguably, one of the most striking shortcomings of this model class compared to robust human perception. A successful method to increase adversarial robustness is *adversarial training* [e.g. 48, 49]. The resulting models were found to transfer better, have meaningful gradients [50], and enable interpolating between two input images [51]: “robust optimization can actually be viewed as inducing a *human prior* over the features that models are able to learn” [52, p. 10]. Therefore, we include five models with a ResNet-50 architecture and different accuracy-robustness tradeoffs, adversarially trained on ImageNet with Microsoft-scale resources by [32] to test whether models with “perceptually-aligned representations” also show human-aligned OOD generalisation behaviour—as we would hope. This is not the case: the stronger the model is trained adversarially (darker shades of blue in Figure 2), the more susceptible it becomes to (random) image degradations. Most strikingly, a simple rotation by 90 degrees leads to a 50% drop in classification accuracy. Adversarial robustness seems to come at the cost of increased vulnerability to large-scale perturbations.⁶ On the other hand, there is a silver lining: when testing whether models are biased towards texture or shape by testing them on cue conflict images (Figure 3), in accordance with [54, 55] we observe a perfect relationship between shape bias and the degree of adversarial training, a big step in the direction of human shape bias (and a stronger shape bias than any of the other models).

Vision transformers In computer vision, convolutional networks have become by far the dominating model class over the last decade. Vision transformers [33] break with the long tradition of using convolutions and are rapidly gaining traction [56]. We find that the best vision transformer (ViT-L trained on 14M images) even *exceeds* human OOD accuracy (Figure 1a shows the average across 17 datasets). There appears to be an additive effect of architecture and data: vision transformers trained on 1M images (light green) are already better than standard convolutional models; training on 14M images (dark green) gives another performance boost. In line with [57, 58], we observe a higher shape bias compared to most standard CNNs.

Standard models trained on more data: BiT-M, SWSL, Noisy Student Interestingly, the biggest effect on OOD robustness we find simply comes from training on larger datasets, not from advanced architectures. When standard models are combined with large-scale training (14M images for BiT-M, 300M for Noisy Student and a remarkable 940M for SWSL), OOD accuracies reach levels not known from standard ImageNet-trained models; these models even outperform a more powerful architecture

⁶This might be related to [53], who studied a potentially related tradeoff between selectivity and invariance.

(vision transformer ViT-S) trained on less data (1M) as shown in Figure 1a. Simply training on (substantially) more data substantially narrows the gap to human OOD accuracies (1b).

CLIP CLIP is special: trained on 400M images (more data) with joint language-image supervision (novel objective) and a vision transformer backbone (non-standard architecture), it is the most human-like model across all of our metrics presented in Figure 1; most strikingly in terms of error consistency to humans (which will be discussed in the next section). We tested a number of hypotheses to disentangle why CLIP is “special”. *H1: because CLIP is trained on a lot of data?* No: Noisy Student—a model trained on a comparably large dataset of 300M images—does not perform as well. *H2: because CLIP receives higher-quality labels?* About 6% of ImageNet labels are plainly wrong [59]. Could it be the case that CLIP simply performs better since it doesn’t suffer from this issue? In order to test this, we used CLIP to generate new labels for all 1.3M ImageNet images: (a) hard labels, i.e. the top-1 class predicted by CLIP; and (b) soft labels, i.e. using CLIP’s full posterior distribution as a target. We then trained ResNet-50 from scratch on CLIP hard and soft labels (for details see Appendix D). However, this does not show any robustness improvements over a vanilla ImageNet-trained ResNet-50, thus different/better labels are not a likely root cause. *H3: because CLIP has a special image+text loss?* Yes and no: CLIP training on ResNet-50 leads to astonishingly poor OOD results, so training a standard model with CLIP loss alone is insufficient. However, while neither architecture nor loss alone sufficiently explain why CLIP is special, we find a clear interaction between architecture and loss (described in more detail in the Appendix along with the other “CLIP ablation” experiments mentioned above).

4 Consistency between models: data-rich models narrow the substantial image-level consistency gap between human and machine vision

In the previous section we have seen that while self-supervised and adversarially trained models lack OOD robustness, models based on vision transformers and/or trained on large-scale datasets now match or exceed human performance on most datasets. Behaviourally, a natural follow-up question is to ask not just how many, but *which* errors models make—i.e., do they make errors on the same individual images as humans on OOD data (an important characteristic of a “human-like” model)? This is quantified via *error consistency* (defined in Section 2); which additionally allows us to compare models with each other, asking e.g. which model classes make similar errors. In Figure 4, we compare all models with each other and with humans, asking whether they make errors on the same images. On this particular dataset (sketch images), we can see one big model cluster. Irrespective of whether one takes a standard supervised model, a self-supervised model, an adversarially trained model or a vision transformer, all those models make highly systematic errors (which extends the results of [20, 60] who found similarities between standard vanilla CNNs). Humans, on the other hand, show a very different pattern of errors. Interestingly, the boundary between humans and some data-rich models at the bottom of the figure—especially CLIP (400M images) and SWSL (940M)—is blurry: some (but not all) data-rich models much more closely mirror the patterns of errors that humans make, and we identified the first models to achieve higher error consistency with humans than with other (standard) models. Are these promising results shared across datasets, beyond the sketch images? In Figures 1c and 1d, aggregated results over 17 datasets are presented. Here, we can see that data-rich models approach human-to-human observed consistency, but not error consistency. Taken in isolation, *observed* consistency is not a good measure of image-level consistency since it does not take consistency by chance into account; *error* consistency tracks whether there is consistency beyond chance; here we see that there is still a substantial image-level *consistency gap* between human and machine vision. However, several models improve over vanilla CNNs, especially BiT-M (trained on 14M images) and CLIP (400M images). This progress is non-trivial; at the same time, there is ample room for future improvement.

How do the findings from Figure 4 (showing nearly human-level error consistency for sketch images) and from Figure 1d (showing a substantial consistency gap when aggregating over 17 datasets) fit together? Upon closer inspection, we discovered that there are two distinct cases. On 12 datasets (stylized, colour/greyscale, contrast, high-pass, phase-scrambling, power-equalisation, false colour, rotation, eidolonI, -II and -III as well as uniform noise), the human-machine gap is large; here, more robust models do not show improved error consistency (as can be see in Figure 5a). On the other hand, for five datasets (sketch, silhouette, edge, cue conflict, low-pass filtering), there is a completely different result pattern: Here, OOD accuracy is a near-perfect predictor of error

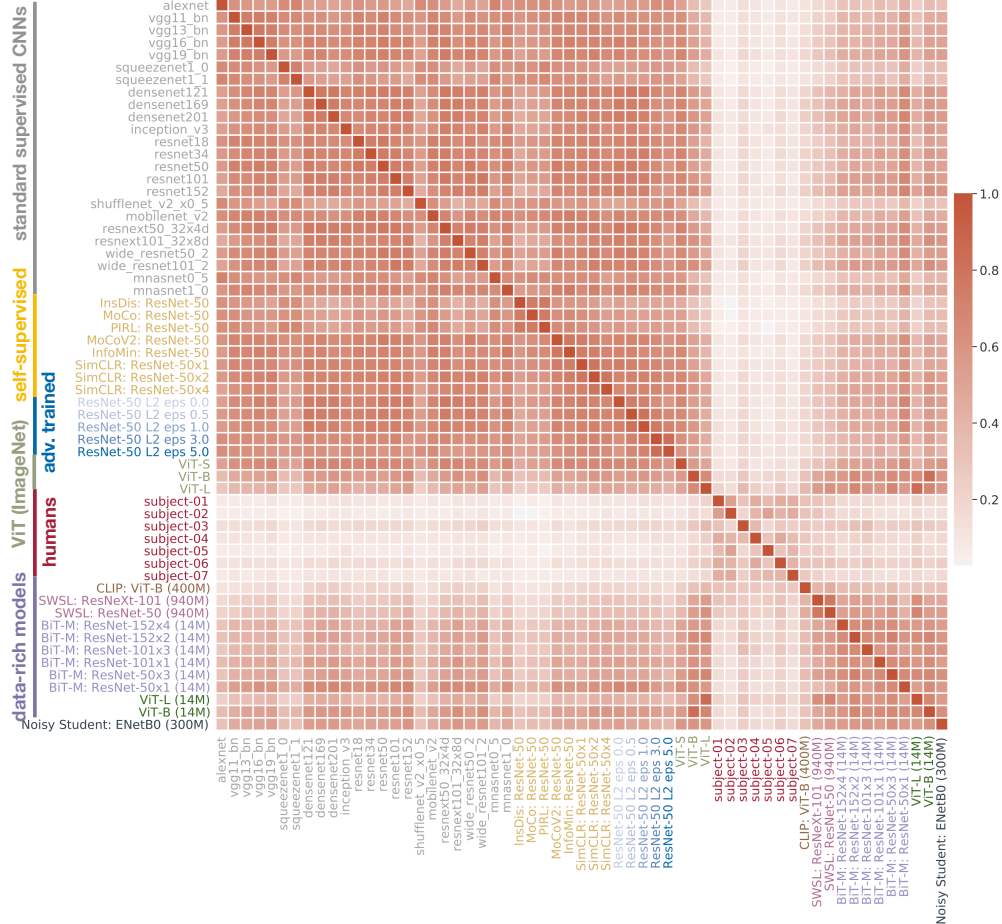


Figure 4: Data-rich models narrow the substantial image-level consistency gap between humans and machines. Error consistency analysis on a single dataset (sketch images; for other datasets see Appendix, Figures 9, 11, 12, 13, 14) shows that most models cluster (dark red = highly consistent errors) irrespective of their architecture and objective function; humans cluster differently (high human-to-human consistency, low human-to-model consistency); but some data-rich models including CLIP and SWSL blur the boundary, making more human-like errors than standard models.

consistency, which means that improved generalisation robustness leads to more human-like errors (Figure 5b). Furthermore, training on large-scale datasets leads to considerable improvements along both axes for standard CNNs. Within models trained on larger datasets, CLIP scores best; but models with a standard architecture (SWSL: based on ResNet-50 and ResNeXt-101) closely follow suit.

It remains an open question why the training dataset appears to have the most important impact on a model’s decision boundary as measured by error consistency (as opposed to other aspects of a model’s inductive bias). Datasets contain various shortcut opportunities [14], and if two different models are trained on similar data, they might converge to a similar solution simply by exploiting the same shortcuts—which would also fit well to the finding that adversarial examples typically transfer very well between different models [61, 62]. Making models more flexible (such as transformers, a generalisation of CNNs) wouldn’t change much in this regard, since flexible models can still exploit the same shortcuts. Two predictions immediately follow from this hypothesis: (1.) error consistency between two identical models trained on very different datasets, such as ImageNet vs. Stylized-ImageNet, is much lower than error consistency between very different models (ResNet-50 vs. VGG-16) trained on the same dataset. (2.) error consistency between ResNet-50 and a highly flexible model (e.g., a vision transformer) is much higher than error consistency between ResNet-50 and a highly constrained model like BagNet-9 [63]. We provide evidence for both predictions in Appendix B, which makes the shortcut hypothesis of model similarity a potential starting point for future analyses.

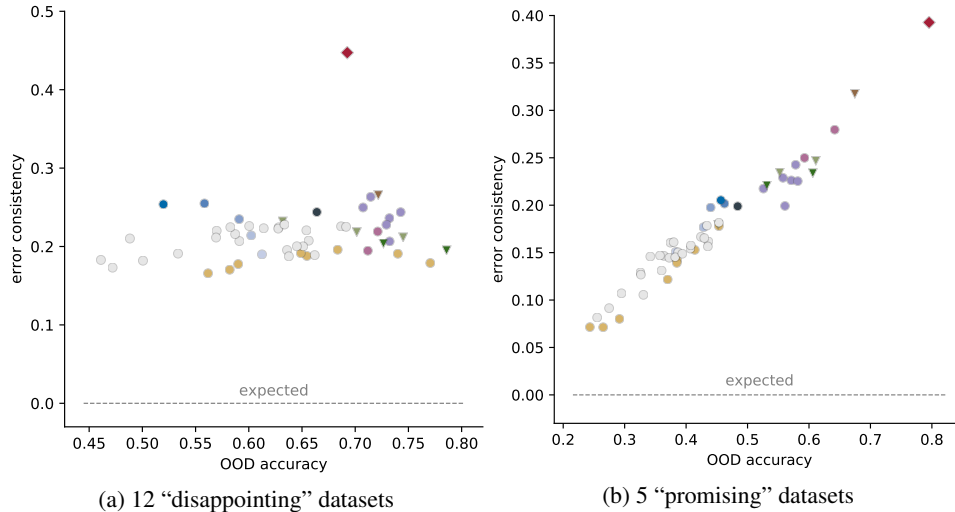


Figure 5: Partial failure, partial success: Error consistency with humans aggregated over multiple datasets. Left: 12 datasets where model accuracies exceed human accuracies; here, there is still a substantial image-level consistency gap to humans. Right: 5 datasets (sketch, silhouette, edge, cue conflict, low-pass) where humans are more robust. Here, OOD accuracy is a near-perfect predictor of image-level consistency; especially data-rich models (e.g. CLIP, SWSL, BiT) narrow the consistency gap to humans. Symbols indicate architecture type (\circ convolutional, ∇ vision transformer, \diamond human).

5 Discussion

Summary We set out to answer the question: *Are we making progress in closing the gap between human and machine vision?* In order to quantify progress, we performed large-scale psychophysical experiments on 17 out-of-distribution datasets (which will be open-sourced along with Python evaluation code as a benchmark to track future progress). We then investigated models that push the boundaries of traditional deep learning (different objective functions, architectures, and dataset sizes ranging from 1M to 1B), asking how they perform relative to human visual perception. We found that the OOD robustness gap between human and machine vision is closing, as the best models now match or exceed human accuracies. At the same time, an image-level consistency gap remains, however, this gap that is at least in some cases narrowing for models trained on large-scale datasets.

Limitations Model robustness is studied from many different viewpoints, including adversarial robustness [61], theoretical robustness guarantees [e.g. 64], or label noise robustness [e.g. 65]. The focus of our study is robustness towards non-adversarial out-of-distribution data, which is particularly well-suited for comparisons with humans. Furthermore, human and machine vision can be compared in many different ways. This includes comparing against neural data [66, 67], contrasting Gestalt effects [e.g. 68], object similarity judgments [69], or mid-level properties [46] and is of course not limited to studying object recognition. By no means do we mean to imply that our behavioural comparison is the only feasible option—on the contrary, we believe it will be all the more exciting to investigate whether our behavioural findings have implications for other means of comparison!

Discussion We have to admit that we view our results concerning the benefits of increasing dataset size by one-to-three orders of magnitude with mixed feelings. On the one hand, “simply” training standard models on (a lot) more data certainly has an intellectually disappointing element—particularly given many rich ideas in the cognitive science and neuroscience literature on which architectural changes might be required to bring machine vision closer to human vision [70–75]. Additionally, large-scale training comes with infrastructure demands that are hard to meet for many academic researchers. On the other hand, we find it truly exciting to see that machine models are narrowing not just the OOD robustness gap to humans, but that also, at least for some datasets, those models are actually making more human-like decisions on an individual image level; image-level response consistency is a much stricter behavioural requirement than just e.g. matching overall accuracies. Taken together, our results give reason to celebrate partial success in closing the gap between human and machine vision. In those cases where there is still ample room for improvement, our psychophysical benchmark datasets and library may prove useful in quantifying future progress.

Acknowledgments and disclosure of funding

We thank Simon Kornblith, Kristof Meding, Claudio Michaelis and Ludwig Schmidt for helpful discussions regarding different aspects of this work; Lukas Huber, Maximus Mutschler, David-Elias Künstle for feedback on the manuscript; Santiago Cadena for sharing a PyTorch implementation of SimCLR; Katherine Hermann and her collaborators for providing supervised SimCLR baselines; Uli Wannek and Silke Gramer for infrastructure/administrative support and the many authors who made their models publicly available.

Furthermore, we are grateful to the International Max Planck Research School for Intelligent Systems (IMPRS-IS) for supporting R.G.; the Collaborative Research Center (Projektnummer 276693517—SFB 1233: Robust Vision) for supporting M.B. and F.A.W.; the German Federal Ministry of Education and Research through the Tübingen AI Center (FKZ 01IS18039A) for supporting W.B. and M.B.; and the German Research Foundation through the Cluster of Excellence “Machine Learning—New Perspectives for Science”, EXC 2064/1 for supporting F.A.W. (project number 390727645). M.B. and W.B. acknowledge funding from the MICrONS program of the Intelligence Advanced Research Projects Activity (IARPA) via Department of Interior/Interior Business Center (DoI/IBC) contract number D16PC00003.

Author contributions

Project idea: R.G. and W.B.; project lead: R.G.; coding toolbox and model evaluation pipeline: R.G., K.N. and B.M. based on a prototype by R.G.; training models: K.N. with input from R.G., W.B. and M.B.; data visualisation: R.G., B.M. and K.N. with input from M.B., F.A.W. and W.B.; psychophysical data collection: T.T. (12 datasets) and B.M. (2 datasets) under the guidance of R.G. and F.A.W.; curating stimuli: R.G.; interpreting analyses and findings: R.G., M.B., F.A.W. and W.B.; guidance, feedback, infrastructure & funding acquisition: M.B., F.A.W. and W.B.; paper writing: R.G. with help from F.A.W. and W.B. and input from all other authors.

References

- [1] Alex Krizhevsky, Ilya Sutskever, and Geoffrey E Hinton. ImageNet classification with deep convolutional neural networks. In *Advances in Neural Information Processing Systems*, pages 1097–1105, 2012.
- [2] Jinjiang Wang, Yulin Ma, Laibin Zhang, Robert X Gao, and Dazhong Wu. Deep learning for smart manufacturing: Methods and applications. *Journal of Manufacturing Systems*, 48:144–156, 2018.
- [3] Javier Villalba-Diez, Daniel Schmidt, Roman Gevers, Joaquín Ordieres-Meré, Martin Buchwitz, and Wanja Wellbrock. Deep learning for industrial computer vision quality control in the printing industry 4.0. *Sensors*, 19(18):3987, 2019.
- [4] Christof Angermueller, Tanel Pärnamaa, Leopold Parts, and Oliver Stegle. Deep learning for computational biology. *Molecular Systems Biology*, 12(7):878, 2016.
- [5] Adam H Marblestone, Greg Wayne, and Konrad P Kording. Toward an integration of deep learning and neuroscience. *Frontiers in Computational Neuroscience*, 10:94, 2016.
- [6] Garrett B Goh, Nathan O Hodas, and Abhinav Vishnu. Deep learning for computational chemistry. *Journal of Computational Chemistry*, 38(16):1291–1307, 2017.
- [7] Travers Ching, Daniel S Himmelstein, Brett K Beaulieu-Jones, Alexandr A Kalinin, Brian T Do, Gregory P Way, Enrico Ferrero, Paul-Michael Agapow, Michael Zietz, Michael M Hoffman, et al. Opportunities and obstacles for deep learning in biology and medicine. *Journal of The Royal Society Interface*, 15(141):20170387, 2018.
- [8] Dan Guest, Kyle Cranmer, and Daniel Whiteson. Deep learning and its application to LHC physics. *Annual Review of Nuclear and Particle Science*, 68:161–181, 2018.
- [9] Andrew W Senior, Richard Evans, John Jumper, James Kirkpatrick, Laurent Sifre, Tim Green, Chongli Qin, Augustin Žídek, Alexander WR Nelson, Alex Bridgland, et al. Improved protein structure prediction using potentials from deep learning. *Nature*, 577(7792):706–710, 2020.
- [10] Olga Russakovsky, Jia Deng, Hao Su, Jonathan Krause, Sanjeev Satheesh, Sean Ma, Zhiheng Huang, Andrej Karpathy, Aditya Khosla, Michael Bernstein, Alexander C Berg, and Li Fei-Fei. ImageNet Large Scale Visual Recognition Challenge. *International Journal of Computer Vision*, 115(3):211–252, 2015.
- [11] Jason Jo and Yoshua Bengio. Measuring the tendency of cnns to learn surface statistical regularities. *arXiv preprint arXiv:1711.11561*, 2017.
- [12] Sara Beery, Grant Van Horn, and Pietro Perona. Recognition in terra incognita. In *Proceedings of the European Conference on Computer Vision*, pages 456–473, 2018.

- [13] Timothy Niven and Hung-Yu Kao. Probing neural network comprehension of natural language arguments. In *Proceedings of the 57th Annual Meeting of the Association for Computational Linguistics*, pages 4658–4664, 2019.
- [14] Robert Geirhos, Jörn-Henrik Jacobsen, Claudio Michaelis, Richard Zemel, Wieland Brendel, Matthias Bethge, and Felix A Wichmann. Shortcut learning in deep neural networks. *Nature Machine Intelligence*, 2:665–673, 2020.
- [15] Dan Hendrycks and Thomas Dietterich. Benchmarking neural network robustness to common corruptions and perturbations. In *International Conference on Learning Representations*, 2019.
- [16] Haohan Wang, Songwei Ge, Eric P Xing, and Zachary C Lipton. Learning robust global representations by penalizing local predictive power. *arXiv preprint arXiv:1905.13549*, 2019.
- [17] Robert Geirhos, Patricia Rubisch, Claudio Michaelis, Matthias Bethge, Felix A. Wichmann, and Wieland Brendel. ImageNet-trained CNNs are biased towards texture; increasing shape bias improves accuracy and robustness. In *International Conference on Learning Representations*, 2019.
- [18] David M. Green. Consistency of auditory detection judgments. *Psychological Review*, 71(5):392–407, 1964.
- [19] Kristof Meding, Dominik Janzing, Bernhard Schölkopf, and Felix A. Wichmann. Perceiving the arrow of time in autoregressive motion. *Advances in Neural Information Processing Systems (NeurIPS)*, 32: 2303–2314, 2019.
- [20] Robert Geirhos, Kristof Meding, and Felix A Wichmann. Beyond accuracy: quantifying trial-by-trial behaviour of CNNs and humans by measuring error consistency. *Advances in Neural Information Processing Systems*, 33, 2020.
- [21] Robert Geirhos, Carlos RM Temme, Jonas Rauber, Heiko H Schütt, Matthias Bethge, and Felix A Wichmann. Generalisation in humans and deep neural networks. In *Advances in Neural Information Processing Systems*, 2018.
- [22] George A Miller. WordNet: a lexical database for English. *Communications of the ACM*, 38(11):39–41, 1995.
- [23] Sébastien Marcel and Yann Rodriguez. Torchvision the machine-vision package of torch. In *Proceedings of the 18th ACM International Conference on Multimedia*, pages 1485–1488, 2010.
- [24] Zhirong Wu, Yuanjun Xiong, Stella X Yu, and Dahua Lin. Unsupervised feature learning via non-parametric instance discrimination. In *Proceedings of the IEEE Conference on Computer Vision and Pattern Recognition*, pages 3733–3742, 2018.
- [25] Kaiming He, Haoqi Fan, Yuxin Wu, Saining Xie, and Ross Girshick. Momentum contrast for unsupervised visual representation learning. In *Proceedings of the IEEE Conference on Computer Vision and Pattern Recognition*, pages 9729–9738, 2020.
- [26] Xinlei Chen, Haoqi Fan, Ross Girshick, and Kaiming He. Improved baselines with momentum contrastive learning. *arXiv preprint arXiv:2003.04297*, 2020.
- [27] Ishan Misra and Laurens van der Maaten. Self-supervised learning of pretext-invariant representations. In *Proceedings of the IEEE Conference on Computer Vision and Pattern Recognition*, pages 6707–6717, 2020.
- [28] Yonglong Tian, Chen Sun, Ben Poole, Dilip Krishnan, Cordelia Schmid, and Phillip Isola. What makes for good views for contrastive learning. *arXiv preprint arXiv:2005.10243*, 2020.
- [29] Ting Chen, Simon Kornblith, Mohammad Norouzi, and Geoffrey Hinton. A simple framework for contrastive learning of visual representations. *arXiv preprint arXiv:2002.05709*, 2020.
- [30] Robert Geirhos, Kantharaju Narayanappa, Benjamin Mitzkus, Matthias Bethge, Felix A Wichmann, and Wieland Brendel. On the surprising similarities between supervised and self-supervised models. *arXiv preprint arXiv:2010.08377*, 2020.
- [31] Alexander Kolesnikov, Lucas Beyer, Xiaohua Zhai, Joan Puigcerver, Jessica Yung, Sylvain Gelly, and Neil Houlsby. Big transfer (BiT): General visual representation learning. *arXiv preprint arXiv:1912.11370*, 6(2):8, 2019.

- [32] Hadi Salman, Andrew Ilyas, Logan Engstrom, Ashish Kapoor, and Aleksander Madry. Do adversarially robust ImageNet models transfer better? *arXiv preprint arXiv:2007.08489*, 2020.
- [33] Alexey Dosovitskiy, Lucas Beyer, Alexander Kolesnikov, Dirk Weissenborn, Xiaohua Zhai, Thomas Unterthiner, Mostafa Dehghani, Matthias Minderer, Georg Heigold, Sylvain Gelly, et al. An image is worth 16x16 words: Transformers for image recognition at scale. *arXiv preprint arXiv:2010.11929*, 2020.
- [34] Ross Wightman. PyTorch image models. <https://github.com/rwightman/pytorch-image-models>, 2019.
- [35] I Zeki Yalniz, Hervé Jégou, Kan Chen, Manohar Paluri, and Dhruv Mahajan. Billion-scale semi-supervised learning for image classification. *arXiv preprint arXiv:1905.00546*, 2019.
- [36] Qizhe Xie, Minh-Thang Luong, Eduard Hovy, and Quoc V Le. Self-training with noisy student improves ImageNet classification. In *Proceedings of the IEEE Conference on Computer Vision and Pattern Recognition*, pages 10687–10698, 2020.
- [37] Alec Radford, Jong Wook Kim, Chris Hallacy, Aditya Ramesh, Gabriel Goh, Sandhini Agarwal, Girish Sastry, Amanda Askell, Pamela Mishkin, Jack Clark, et al. Learning transferable visual models from natural language supervision. *arXiv preprint arXiv:2103.00020*, 2021.
- [38] Jacob Cohen. A coefficient of agreement for nominal scales. *Educational and Psychological Measurement*, 20(1):37–46, 1960.
- [39] Samuel Dodge and Lina Karam. A study and comparison of human and deep learning recognition performance under visual distortions. In *26th International Conference on Computer Communication and Networks*, pages 1–7. IEEE, 2017.
- [40] Thomas Serre. Deep learning: the good, the bad, and the ugly. *Annual Review of Vision Science*, 5:399–426, 2019.
- [41] Yann LeCun. Predictive learning, 2016. URL <https://www.youtube.com/watch?v=0unt2Y4qxQo>.
- [42] William Lotter, Gabriel Kreiman, and David Cox. A neural network trained for prediction mimics diverse features of biological neurons and perception. *Nature Machine Intelligence*, 2(4):210–219, 2020.
- [43] A Emin Orhan, Vaibhav V Gupta, and Brenden M Lake. Self-supervised learning through the eyes of a child. *arXiv preprint arXiv:2007.16189*, 2020.
- [44] Talia Konkle and George A Alvarez. Instance-level contrastive learning yields human brain-like representation without category-supervision. *bioRxiv*, 2020.
- [45] Chengxu Zhuang, Siming Yan, Aran Nayebi, Martin Schrimpf, Michael Frank, James DiCarlo, and Daniel Yamins. Unsupervised neural network models of the ventral visual stream. *bioRxiv*, 2020.
- [46] Katherine R Storrs, Barton L Anderson, and Roland W Fleming. Unsupervised learning predicts human perception and misperception of gloss. *Nature Human Behaviour*, pages 1–16, 2021.
- [47] Katherine Hermann, Ting Chen, and Simon Kornblith. The origins and prevalence of texture bias in convolutional neural networks. *Advances in Neural Information Processing Systems*, 33, 2020.
- [48] Ian J Goodfellow, Jonathon Shlens, and Christian Szegedy. Explaining and harnessing adversarial examples. *arXiv preprint arXiv:1412.6572*, 2014.
- [49] Ruitong Huang, Bing Xu, Dale Schuurmans, and Csaba Szepesvári. Learning with a strong adversary. *arXiv preprint arXiv:1511.03034*, 2015.
- [50] Simran Kaur, Jeremy Cohen, and Zachary C Lipton. Are perceptually-aligned gradients a general property of robust classifiers? *arXiv preprint arXiv:1910.08640*, 2019.
- [51] Shibani Santurkar, Dimitris Tsipras, Brandon Tran, Andrew Ilyas, Logan Engstrom, and Aleksander Madry. Image synthesis with a single (robust) classifier. *arXiv:1906.09453*, 2019.
- [52] Logan Engstrom, Andrew Ilyas, Shibani Santurkar, Dimitris Tsipras, Brandon Tran, and Aleksander Madry. Adversarial robustness as a prior for learned representations. *arXiv preprint arXiv:1906.00945*, 2019.
- [53] Florian Tramèr, Jens Behrmann, Nicholas Carlini, Nicolas Papernot, and Jörn-Henrik Jacobsen. Fundamental tradeoffs between invariance and sensitivity to adversarial perturbations. In *International Conference on Machine Learning*, pages 9561–9571. PMLR, 2020.

- [54] Tianyuan Zhang and Zhanxing Zhu. Interpreting adversarially trained convolutional neural networks. In *International Conference on Machine Learning*, pages 7502–7511. PMLR, 2019.
- [55] Peijie Chen, Chirag Agarwal, and Anh Nguyen. The shape and simplicity biases of adversarially robust ImageNet-trained CNNs. *arXiv preprint arXiv:2006.09373*, 2020.
- [56] Kai Han, Yunhe Wang, Hanting Chen, Xinghao Chen, Jianyuan Guo, Zhenhua Liu, Yehui Tang, An Xiao, Chunjing Xu, Yixing Xu, et al. A survey on visual transformer. *arXiv preprint arXiv:2012.12556*, 2020.
- [57] Muzammal Naseer, Kanchana Ranasinghe, Salman Khan, Munawar Hayat, Fahad Shahbaz Khan, and Ming-Hsuan Yang. Intriguing properties of vision transformers. *arXiv preprint arXiv:2105.10497*, 2021.
- [58] Shikhar Tuli, Ishita Dasgupta, Erin Grant, and Thomas L Griffiths. Are convolutional neural networks or transformers more like human vision? *arXiv preprint arXiv:2105.07197*, 2021.
- [59] Curtis G Northcutt, Anish Athalye, and Jonas Mueller. Pervasive label errors in test sets destabilize machine learning benchmarks. *arXiv preprint arXiv:2103.14749*, 2021.
- [60] Horia Mania, John Miller, Ludwig Schmidt, Moritz Hardt, and Benjamin Recht. Model similarity mitigates test set overuse. *Advances in Neural Information Processing Systems*, 2019.
- [61] Christian Szegedy, Wojciech Zaremba, Ilya Sutskever, Joan Bruna, Dumitru Erhan, Ian Goodfellow, and Rob Fergus. Intriguing properties of neural networks. *arXiv:1312.6199*, 2013.
- [62] Florian Tramèr, Nicolas Papernot, Ian Goodfellow, Dan Boneh, and Patrick McDaniel. The space of transferable adversarial examples. *arXiv preprint arXiv:1704.03453*, 2017.
- [63] Wieland Brendel and Matthias Bethge. Approximating CNNs with bag-of-local-features models works surprisingly well on ImageNet. In *International Conference on Learning Representations*, 2019.
- [64] Matthias Hein and Maksym Andriushchenko. Formal guarantees on the robustness of a classifier against adversarial manipulation. *arXiv preprint arXiv:1705.08475*, 2017.
- [65] Arash Vahdat. Toward robustness against label noise in training deep discriminative neural networks. *arXiv preprint arXiv:1706.00038*, 2017.
- [66] Daniel LK Yamins, Ha Hong, Charles F Cadieu, Ethan A Solomon, Darren Seibert, and James J DiCarlo. Performance-optimized hierarchical models predict neural responses in higher visual cortex. *Proceedings of the National Academy of Sciences*, 111(23):8619–8624, 2014.
- [67] Jonas Kubilius, Martin Schrimpf, Kohitij Kar, Rishi Rajalingham, Ha Hong, Najib Majaj, Elias Issa, Pouya Bashivan, Jonathan Prescott-Roy, Kailyn Schmidt, et al. Brain-like object recognition with high-performing shallow recurrent ANNs. *Advances in Neural Information Processing Systems*, 32:12805–12816, 2019.
- [68] Been Kim, Emily Reif, Martin Wattenberg, Samy Bengio, and Michael C Mozer. Neural networks trained on natural scenes exhibit Gestalt closure. *Computational Brain & Behavior*, pages 1–13, 2021.
- [69] Martin N Hebart, Charles Y Zheng, Francisco Pereira, and Chris I Baker. Revealing the multidimensional mental representations of natural objects underlying human similarity judgements. *Nature Human Behaviour*, 4(11):1173–1185, 2020.
- [70] Nikolaus Kriegeskorte. Deep neural networks: a new framework for modeling biological vision and brain information processing. *Annual Review of Vision Science*, 1:417–446, 2015.
- [71] Brenden M Lake, Tomer D Ullman, Joshua B Tenenbaum, and Samuel J Gershman. Building machines that learn and think like people. *Behavioral and Brain Sciences*, 40, 2017.
- [72] Amirhossein Tavanaei, Masoud Ghodrati, Saeed Reza Kheradpisheh, Timothée Masquelier, and Anthony Maida. Deep learning in spiking neural networks. *Neural Networks*, 111:47–63, 2019.
- [73] Fabian H Sinz, Xaq Pitkow, Jacob Reimer, Matthias Bethge, and Andreas S Tolias. Engineering a less artificial intelligence. *Neuron*, 103(6):967–979, 2019.
- [74] Joel Dapello, Tiago Marques, Martin Schrimpf, Franziska Geiger, David D Cox, and James J DiCarlo. Simulating a primary visual cortex at the front of CNNs improves robustness to image perturbations. *bioRxiv*, 2020.
- [75] Benjamin D Evans, Gaurav Malhotra, and Jeffrey S Bowers. Biological convolutions improve dnn robustness to noise and generalisation. *bioRxiv*, 2021.

- [76] Adam Paszke, Sam Gross, Francisco Massa, Adam Lerer, James Bradbury, Gregory Chanan, Trevor Killeen, Zeming Lin, Natalia Gimelshein, Luca Antiga, et al. PyTorch: An imperative style, high-performance deep learning library. In *Advances in Neural Information Processing Systems*, pages 8026–8037, 2019.
- [77] Aaron van den Oord, Yazhe Li, and Oriol Vinyals. Representation learning with contrastive predictive coding. *arXiv:1807.03748*, 2018.
- [78] Jia Deng, Wei Dong, Richard Socher, Li-Jia Li, Kai Li, and Li Fei-Fei. ImageNet: a large-scale hierarchical image database. In *IEEE Conference on Computer Vision and Pattern Recognition*, pages 248–255, 2009.

Appendix

We here provide details on models (A), describe additional predictions and experiments regarding error consistency mentioned in Section 4 (B), report experimental details regarding our psychophysical experiments (C) and regarding training with ImageNet labels provided by CLIP (D), describe experiments with supervised SimCLR baseline models (E), and provide overall benchmark scores ranking different models (F).

Stimuli are visualized in Figures 7 and 8.

A Python library, “modelvs-human”, to test and benchmark models against high-quality human psychophysical data is available from <https://github.com/bethgelab/model-vs-human/>.

A Model details

Standard supervised models. We used all 24 available pre-trained models from the PyTorch model zoo version 1.4.0 (VGG: with batch norm).

Self-supervised models. InsDis [24], MoCo [25], MoCoV2 [26], PIRL [27] and InfoMin [28] were obtained as pre-trained models from the PyContrast model zoo. We trained one linear classifier per model on top of the self-supervised representation. A PyTorch [76] implementation of SimCLR [29] was obtained via simclr-converter. All self-supervised models use a ResNet-50 architecture and a different training approach within the framework of contrastive learning [e.g. 77].

Adversarially trained models. We obtained five adversarially trained models [32] from the robust-models-transfer repository. All of them have a ResNet-50 architecture, but a different accuracy-L2-robustness tradeoff indicated by ϵ . Here are the five models that we used, in increasing order of adversarial robustness: $\epsilon = 0, 0.5, 1.0, 3.0, 5.0$.

Vision transformers. Three ImageNet-trained vision transformer (ViT) models [33] were obtained from pytorch-image-models [34]. Specifically, we used vit_small_patch16_224, vit_base_patch16_224 and vit_large_patch16_224. They are referred to as ViT-S, ViT-B and ViT-L throughout the paper. Additionally, we included two transformers that were pre-trained on ImageNet21K [78], i.e. 14M images with some 21K classes, before they were fine-tuned on “standard” ImageNet-1K. These two models are referred to as ViT-L (14M) and ViT-B (14M) in the paper. They were obtained from the PyTorch-Pretrained-ViT repository, where they are called L_16_imagenet1k and B_16_imagenet1k. (No ViT-S model was available from the repository.) Note that the “imagenet1k” suffix in the model names does not mean the model was only trained on ImageNet1K. On the contrary, this indicates fine-tuning on ImageNet; as mentioned above these models were pre-trained on ImageNet21K before fine-tuning.

CLIP. OpenAI trained a variety of CLIP models using different backbone networks [37]. Unfortunately, the best-performing model has not been released so far, and it is not currently clear whether it will be released at some point according to issue #2 of OpenAI’s CLIP github repository. We included the most powerful released model in our analysis, a model with a ViT-B/32 backbone.

SWSL Two pre-trained SWSL (semi-weakly supervised) models were obtained from semi-supervised-ImageNet1K-models, one with a ResNet-50 architecture and one with a ResNeXt101_32x16d architecture.

BiT-M Six pre-trained Big Transfer models were obtained from pytorch-image-models [34], where they are called resnetv2_50x1_bitm, resnetv2_50x3_bitm, resnetv2_101x1_bitm, resnetv2_101x3_bitm, resnetv2_152x2_bitm and resnetv2_152x4_bitm.

Noisy Student One pre-trained Noisy Student model was obtained from pytorch-image-models [34], where the model is called tf_efficientnet_b0_ns.

Linear classifier training procedure. The PyContrast repository by Yonglong Tian contains a Pytorch implementation of unsupervised representation learning methods, including pre-trained representation weights. The repository provides training and evaluation pipelines, but it supports only multi-node distributed training and does not (currently) provide weights for the classifier. We have used the repository’s linear classifier evaluation pipeline to train classifiers for InsDis [24], MoCo [25], MoCoV2 [26], PIRL [27] and InfoMin [28] on ImageNet. Pre-trained weights of the model representations (without classifier) were taken from the provided Dropbox link and we then ran the training pipeline on a NVIDIA TESLA P100 using the default parameters configured in the pipeline. Detailed documentation about running the pipeline and parameters can be found in the PyContrast repository (commit #3541b82).

B Error consistency predictions

Table 1: Error consistency across all five non-parametric datasets. Specifically, this comparison compares the influence of dataset vs. architecture (top) and the influence of flexibility vs. constraints (bottom). Results are described in Section B.

	sketch	stylized	edge	silhouette	cue conflict
ResNet-50 vs. VGG-16	0.74	0.56	0.68	0.71	0.59
ResNet-50 vs. ResNet-50 trained on Stylized-ImageNet	0.44	0.09	0.10	0.67	0.27
ResNet-50 vs. vision transformer (ViT-S)	0.67	0.43	0.41	0.68	0.48
ResNet-50 vs. BagNet-9	0.31	0.17	0.32	0.14	0.44

In Section 4, we hypothesised that shortcut opportunities in the dataset may be a potential underlying cause of high error consistency between models, since all sufficiently flexible models will pick up on those same shortcuts. We then made two predictions which we test here.

Dataset vs. architecture. *Prediction:* error consistency between two identical models trained on very different datasets, such as ImageNet vs. Stylized-ImageNet, is much lower than error consistency between very different models (ResNet-50 vs. VGG-16) trained on the same dataset. *Observation:* According to Table 1, this is indeed the case—training ResNet-50 on a different dataset, Stylized-ImageNet [17], leads to lower error consistency than comparing two ImageNet-trained CNNs with different architecture. While this relationship is not perfect (e.g., the difference is small for silhouette images), we have confirmed that this is a general pattern not limited to the specific networks in the table.

Flexibility vs. constraints. *Prediction:* error consistency between ResNet-50 and a highly flexible model (e.g., a vision transformer) is much higher than error consistency between ResNet-50 and a highly constrained model like BagNet-9 [63]. *Observation:* A vision transformer (ViT-S) indeed shows higher error consistency with ResNet-50 than with BagNet-9 (see Table 1). However, this difference is not large for one out of five datasets (cue conflict). One could imagine different reasons for this: perhaps BagNet-9 is still flexible enough to learn a decision rule close to the one of standard ResNet-50 for cue conflict images; and of course there is also the possibility that the hypothesis is wrong. Further insights could be gained by testing successively more constrained versions of the same base model.

C Experimental details regarding psychophysical experiments

C.1 Participant instructions and preparation

Participants were explained how to respond (via mouse click), instructed to respond as accurately as possible, and to go with their best guess if unsure. In order to rule out any potential misunderstanding, participants were asked to name all 16 categories on the response screen. Prior to the experiment, visual acuity was measured with a Snellen chart to ensure normal or corrected to normal vision. Furthermore, four blocks of 80 practice trials each (320 practice trials in total) on undistorted colour or greyscale images were conducted (non-overlapping with experimental stimuli) to gain familiarity with the task. During practice trials, but not experimental trials, visual and auditory feedback was provided: the correct category was highlighted and a “beep” sound was played for incorrect or missed trials. The experiment itself consisted of blocks of 80 trials each, after each blocks participants were free to take a break. In order to increase participant motivation, aggregated performance over the last block was displayed on the screen.

C.2 Participant risks

Our experiment was a standard perceptual experiment, for which no IRB approval was required. The task consisted of viewing corrupted images and clicking with a computer mouse. In order to limit participant risks related to a COVID-19 infection, we implemented the following measures: (1.) The experimenter was tested for corona twice per week. (2.) Prior to participation in our experiments, participants were explained that they could perform a (cost-free) corona test next to our building, and that if they choose to do so, we would pay them 10€/hour for the time spent doing the test and waiting for the result (usually approx. 15–30min). (3.) Experimenter and participant adhered to a strict distance of at least 1.5m during the entire course of the experiment, including instructions and practice trials. During the experiment itself, the participant was the only person in the room; the experimenter was seated in an adjacent room. (4.) Wearing a medical mask was mandatory for both experimenter and participant. (5.) Participants were asked to disinfect their hands prior to the experiment; additionally the desk, mouse etc. were disinfected after completion of an experiment. (6.) Participants were tested in a room where high-performance ventilation was installed; in order to ensure that the ventilation was working as expected we performed a one-time safety check measuring CO₂ parts-per-million before we decided to go ahead with the experiments.

C.3 Participant remuneration

Participants were paid 10€ per hour or granted course credit. Additionally, an incentive bonus of up to 15€ could be earned on top of the standard remuneration. This was meant to further motivate our participants to achieve their optimal performance. The minimum performance for receiving a bonus was set as 15% below the mean of the previous experiments accuracy. The bonus then was linearly calculated with the maximal bonus being given from 15% above the previous experiments mean. The total amount spent on participant compensation amounts to 647,50€.

D Training with CLIP labels

As CLIP performed very well across metrics, we intended to obtain a better understanding for why this might be the case. One hypothesis is that CLIP might just receive better labels: About 6% of ImageNet validation images are mis-labeled according to Northcutt et al. [59]. We therefore designed an experiment where we re-labeled the entire ImageNet training and validation dataset using CLIP predictions as ground truth. Having re-labeled ImageNet, we then trained a standard ResNet-50 model from scratch on this dataset using the standard PyTorch ImageNet training script. Training was performed on-premise cloud using four RTX 2080 Ti GPUs for five days. We ran the training pipeline in distributed mode with an ncl backed using the default parameters configured in the script, except for the number of workers which we changed to 25. Cross-entropy loss was used to train two models, once with CLIP hard labels (the top-1 class predicted by CLIP) and once with CLIP soft labels (using CLIP’s full posterior distribution as training target). The accuracies on the original ImageNet validation dataset of the resulting models ResNet50-CLIP-hard-labels and ResNet-50-CLIP-soft-labels are 63.53 (top-1), 86.97 (top-5) and 64.63 (top-1), 88.60 (top-5) respectively. In

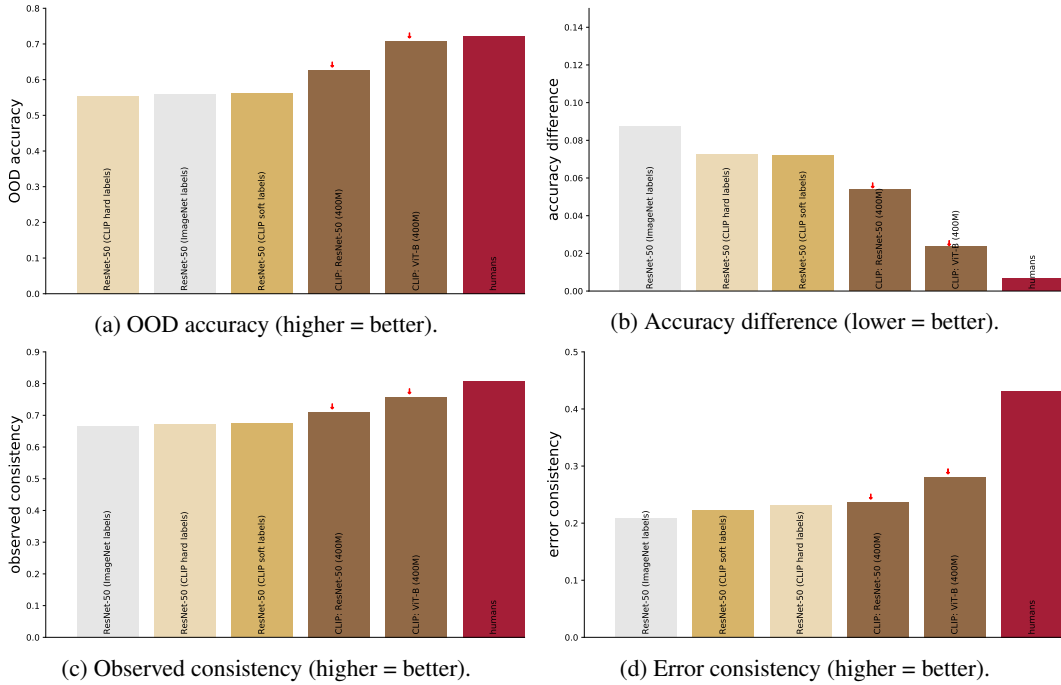


Figure 6: Aggregated results comparing models with and without CLIP-provided labels. Comparison of standard ResNet-50 (light grey), CLIP with vision transformer backend (brown), CLIP with ResNet-50 backend (brown), and standard ResNet-50 with hard labels (bright yellow) vs. soft labels (dark yellow) provided by evaluating standard CLIP on ImageNet; as well as humans (red diamonds) for comparison. Detailed performance across datasets in Figure 16.

order to make sure that the model trained on soft labels had indeed learned to approximate CLIP’s posterior distribution on ImageNet, we calculated the KL divergence between CLIP soft labels and probability distributions from ResNet-50 trained on the CLIP soft labels. The resulting value of 0.001 on both ImageNet training and validation dataset is sufficiently small to conclude that the model had successfully learned to approximate CLIP’s posterior distribution on ImageNet. The results are visualised in Figure 6. The results indicate that simply training a standard ResNet-50 model with labels provided by CLIP does not lead to strong improvements on any metric, which means that ImageNet label errors are unlikely to hold standard models back in terms of OOD accuracy and consistency with human responses.

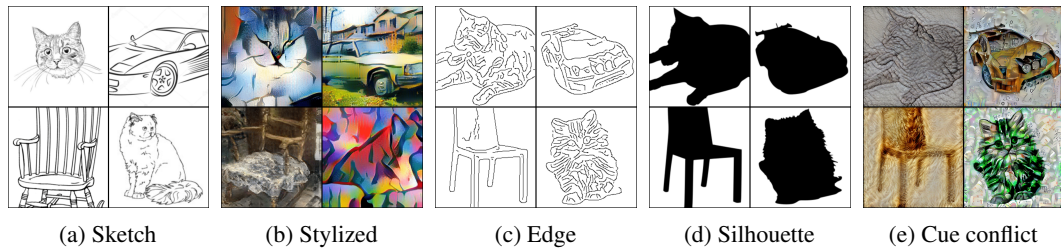


Figure 7: Exemplary stimuli (nonparametric image manipulations) for the following datasets: sketch (7 observers, 800 trials each), stylized (5 observers, 800 trials each), edge (10 observers, 160 trials each), silhouette (10 observers, 160 trials each), and cue conflict (10 observers, 1280 trials each). Figures c–e reprinted from [20] with permission from the authors.

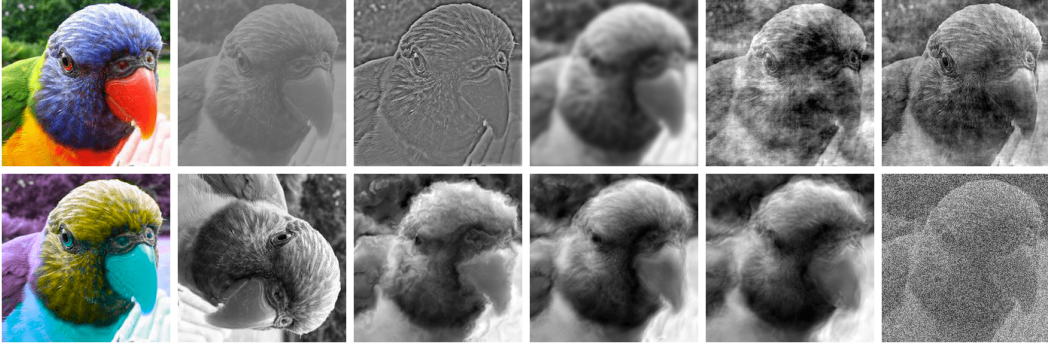


Figure 8: Exemplary stimuli (parametric image manipulations). Manipulations are either binary (e.g. colour vs. grayscale) or they have a parameter (such as the degree of rotation, or the contrast level). Top row: colour vs. grayscale (4 observers, 1280 trials each), low contrast (4 observers, 1280 trials each), high-pass (4 observers, 1280 trials each), low-pass/blurring (4 observers, 1280 trials each), phase noise (4 observers, 1120 trials each), true power spectrum vs. power equalisation (4 observers, 1120 trials each). Bottom row: true vs. opponent colour (4 observers, 1120 trials each), rotation (4 observers, 1280 trials each), Eidolon I (4 observers, 1280 trials each), Eidolon II (4 observers, 1280 trials each), Eidolon III (4 observers, 1280 trials each), additive uniform noise (4 observers, 1280 trials each). Figure adapted from [21] with permission from the authors.

E Supervised SimCLR baseline models

Figure 15 compares the noise generalisation performance self-supervised SimCLR models against augmentation-matched baseline models. The results indicate that the superior performance of SimCLR in Figure 2 are largely a consequence of SimCLR’s data augmentation scheme, rather than a property of the self-supervised contrastive loss.

F Benchmark scores

Figure 1 in the main paper shows aggregated scores for the most robust model in terms of OOD accuracy (Figure 1a), and for the most human-like models in terms of accuracy, observed and error consistency (Figures 1b, 1c, 1d). Numerically, these metrics are represented in two tables, ranking the models according to out-of-distribution robustness (Table 3) and human-like behaviour (Table 2). Since the latter is represented by three different metrics (each characterising a distinct aspect), the mean rank across those three metrics is used to obtain a final ordering. The following conditions and datasets influence benchmark scores: For the five nonparametric datasets, all datasets are taken into account. For the twelve parametric datasets, we also take all datasets into account (overall, all 17 datasets are weighted equally); however, we exclude certain conditions for principled reasons. First of all, the easiest condition is always excluded since it does not test out-of-distribution behaviour (e.g., for the contrast experiment, 100% contrast is more of a baseline condition rather than a condition of interest). Furthermore, we exclude all conditions for which human average performance is strictly smaller than 0.2, since e.g. comparisons against human error patterns are futile if humans are randomly guessing since they cannot identify the stimuli anymore. For these reasons, the following conditions are not taken into account when computing the benchmark scores. Colour vs. greyscale experiment: condition “colour”. True vs. false colour experiment: condition “true colour”. Uniform noise experiment: conditions 0.0, 0.6, 0.9. Low-pass experiment: conditions 0, 15, 40. Contrast experiment: conditions 100, 3, 1. High-pass experiment: conditions inf, 0.55, 0.45, 0.4. Eidolon I experiment: conditions 0, 6, 7. Phase noise experiment: conditions 0, 150, 180. Eidolon II experiment: conditions 0, 5, 6, 7. Power-equalisation experiment: condition “original power spectrum”. Eidolon III experiment: conditions 0, 4, 5, 6, 7. Rotation experiment: condition 0.

Table 2: Benchmark table of model results. The three metrics “accuracy difference” “observed consistency” and “error consistency” (plotted in Figure 1) each produce a different model ranking. The mean rank of a model across those three metrics is used to rank the models on our benchmark.

model	accuracy diff. ↓	obs. consistency ↑	error consistency ↑	mean rank ↓
CLIP: ViT-B (400M)	0.023	0.758	0.281	1.000
SWSL: ResNeXt-101 (940M)	0.028	0.752	0.237	3.667
BiT-M: ResNet-101x1 (14M)	0.034	0.733	0.252	4.000
BiT-M: ResNet-152x2 (14M)	0.035	0.737	0.243	4.667
ViT-L	0.033	0.738	0.222	6.667
BiT-M: ResNet-152x4 (14M)	0.035	0.732	0.233	7.333
BiT-M: ResNet-50x1 (14M)	0.042	0.718	0.240	9.000
BiT-M: ResNet-50x3 (14M)	0.040	0.726	0.228	9.000
ViT-L (14M)	0.035	0.744	0.206	9.667
SWSL: ResNet-50 (940M)	0.041	0.727	0.211	11.333
ViT-B	0.044	0.719	0.223	11.667
Noisy Student: ENetB0 (300M)	0.058	0.700	0.231	12.333
BiT-M: ResNet-101x3 (14M)	0.040	0.720	0.204	14.000
ViT-B (14M)	0.049	0.717	0.209	14.667
densenet201	0.060	0.695	0.212	15.333
ViT-S	0.066	0.684	0.216	17.000
densenet169	0.065	0.688	0.207	17.667
inception_v3	0.066	0.677	0.211	18.000
ResNet-50 L2 eps 1.0	0.079	0.669	0.224	21.333
ResNet-50 L2 eps 3.0	0.079	0.663	0.239	22.000
wide_resnet101_2	0.068	0.676	0.187	24.667
SimCLR: ResNet-50x4	0.071	0.698	0.179	25.000
ResNet-50 L2 eps 0.5	0.078	0.668	0.203	25.667
SimCLR: ResNet-50x2	0.073	0.686	0.180	25.667
densenet121	0.077	0.671	0.200	25.667
resnet101	0.074	0.671	0.192	26.000
resnet152	0.077	0.675	0.190	26.000
resnext101_32x8d	0.074	0.674	0.182	27.000
ResNet-50 L2 eps 5.0	0.087	0.649	0.240	27.000
resnet50	0.087	0.665	0.208	29.000
resnet34	0.084	0.662	0.205	29.667
vgg19_bn	0.081	0.660	0.200	30.333
resnext50_32x4d	0.079	0.666	0.184	30.667
SimCLR: ResNet-50x1	0.080	0.667	0.179	32.333
resnet18	0.091	0.648	0.201	35.000
vgg16_bn	0.088	0.651	0.198	35.000
wide_resnet50_2	0.084	0.663	0.176	36.000
MoCoV2: ResNet-50	0.083	0.660	0.177	36.333
mobilenet_v2	0.092	0.645	0.196	37.333
ResNet-50 L2 eps 0.0	0.086	0.654	0.178	37.667
mnasnet1_0	0.092	0.646	0.189	38.667
vgg11_bn	0.106	0.635	0.193	39.000
InfoMin: ResNet-50	0.086	0.659	0.168	39.333
vgg13_bn	0.101	0.631	0.180	41.333
mnasnet0_5	0.110	0.617	0.173	45.333
MoCo: ResNet-50	0.107	0.617	0.149	47.000
alexnet	0.118	0.597	0.165	47.333
squeezenet1_1	0.131	0.593	0.175	48.000
PIRL: ResNet-50	0.119	0.607	0.141	48.667
shufflenet_v2_x0_5	0.126	0.592	0.160	49.333
InsDis: ResNet-50	0.131	0.593	0.138	50.667
squeezenet1_0	0.145	0.574	0.153	51.000

Table 3: Benchmark table of model results (accuracy).

model	OOD accuracy \uparrow	rank \downarrow
ViT-L (14M)	0.73	1.00
CLIP: ViT-B (400M)	0.71	2.00
ViT-L	0.71	3.00
SWSL: ResNeXt-101 (940M)	0.70	4.00
BiT-M: ResNet-152x2 (14M)	0.69	5.00
BiT-M: ResNet-152x4 (14M)	0.69	6.00
BiT-M: ResNet-101x3 (14M)	0.68	7.00
BiT-M: ResNet-50x3 (14M)	0.68	8.00
SimCLR: ResNet-50x4	0.68	9.00
SWSL: ResNet-50 (940M)	0.68	10.00
BiT-M: ResNet-101x1 (14M)	0.67	11.00
ViT-B (14M)	0.67	12.00
ViT-B	0.66	13.00
BiT-M: ResNet-50x1 (14M)	0.65	14.00
SimCLR: ResNet-50x2	0.64	15.00
densenet201	0.62	16.00
densenet169	0.61	17.00
Noisy Student: ENetB0 (300M)	0.61	18.00
SimCLR: ResNet-50x1	0.60	19.00
resnext101_32x8d	0.59	20.00
resnet152	0.58	21.00
wide_resnet101_2	0.58	22.00
resnet101	0.58	23.00
ViT-S	0.58	24.00
densenet121	0.58	25.00
MoCoV2: ResNet-50	0.57	26.00
inception_v3	0.57	27.00
InfoMin: ResNet-50	0.57	28.00
resnext50_32x4d	0.57	29.00
wide_resnet50_2	0.57	30.00
resnet50	0.56	31.00
resnet34	0.55	32.00
ResNet-50 L2 eps 0.5	0.55	33.00
ResNet-50 L2 eps 1.0	0.55	34.00
vgg19_bn	0.55	35.00
ResNet-50 L2 eps 0.0	0.54	36.00
ResNet-50 L2 eps 3.0	0.53	37.00
vgg16_bn	0.53	38.00
mnasnet1_0	0.52	39.00
resnet18	0.52	40.00
mobilenet_v2	0.52	41.00
MoCo: ResNet-50	0.50	42.00
ResNet-50 L2 eps 5.0	0.50	43.00
vgg13_bn	0.50	44.00
vgg11_bn	0.50	45.00
PIRL: ResNet-50	0.49	46.00
mnasnet0_5	0.47	47.00
InsDis: ResNet-50	0.47	48.00
shufflenet_v2_x0_5	0.44	49.00
alexnet	0.43	50.00
squeezenet1_1	0.43	51.00
squeezenet1_0	0.40	52.00

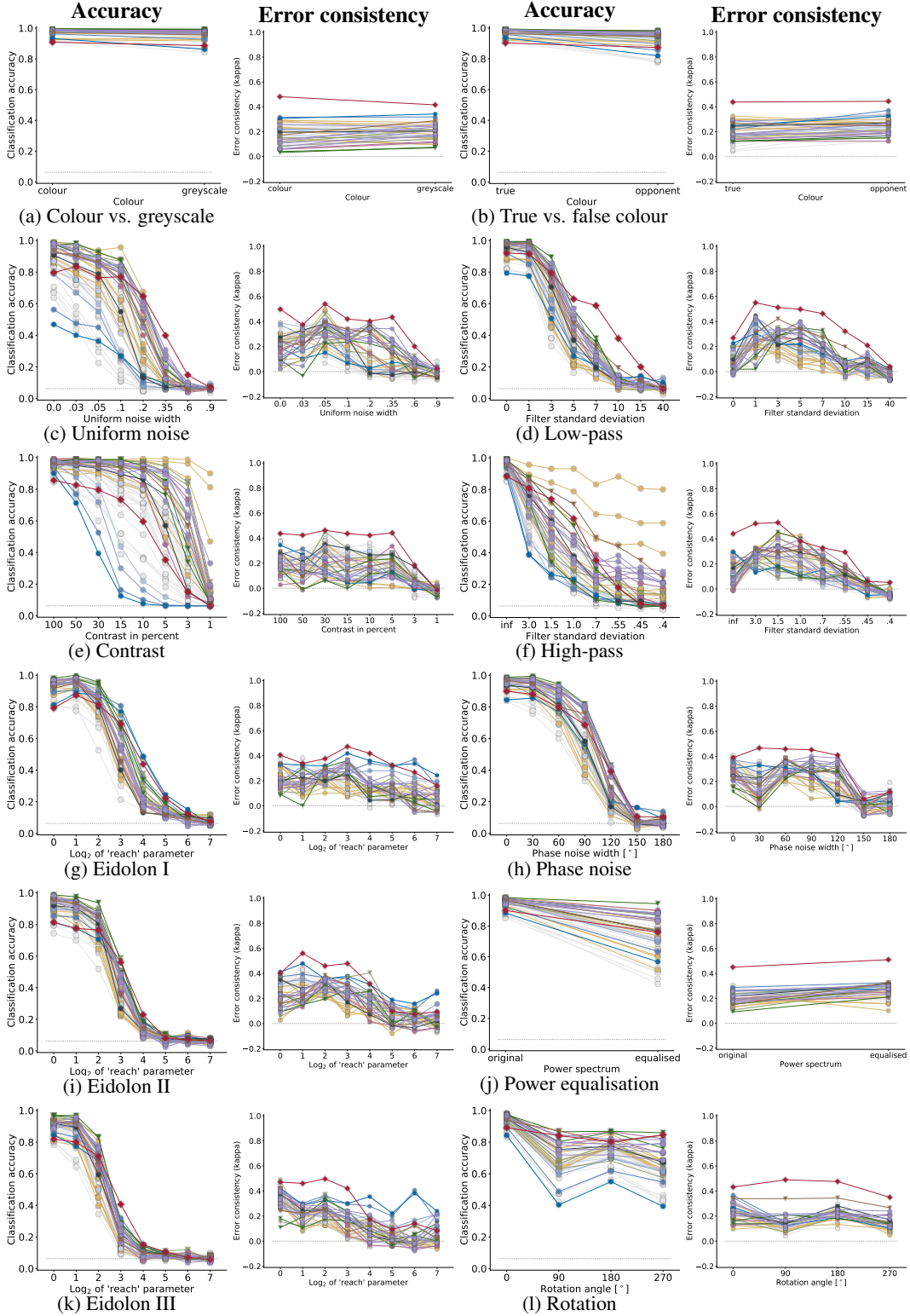


Figure 9: OOD generalisation and error consistency results for **humans**, standard supervised CNNs, **self-supervised models**, **adversarially trained models**, **vision transformers**, noisy student, **BiT**, **SWSL**, **CLIP**. Symbols indicate architecture type (\circ convolutional, ∇ vision transformer, \diamond human); best viewed on screen. ‘Accuracy’ measures recognition performance (higher is better), ‘error consistency’ how closely image-level errors are aligned with humans. Accuracy results identical to Figure 2 in the main paper. In many cases, human-to-human error consistency increases for moderate distortion levels and drops afterwards.

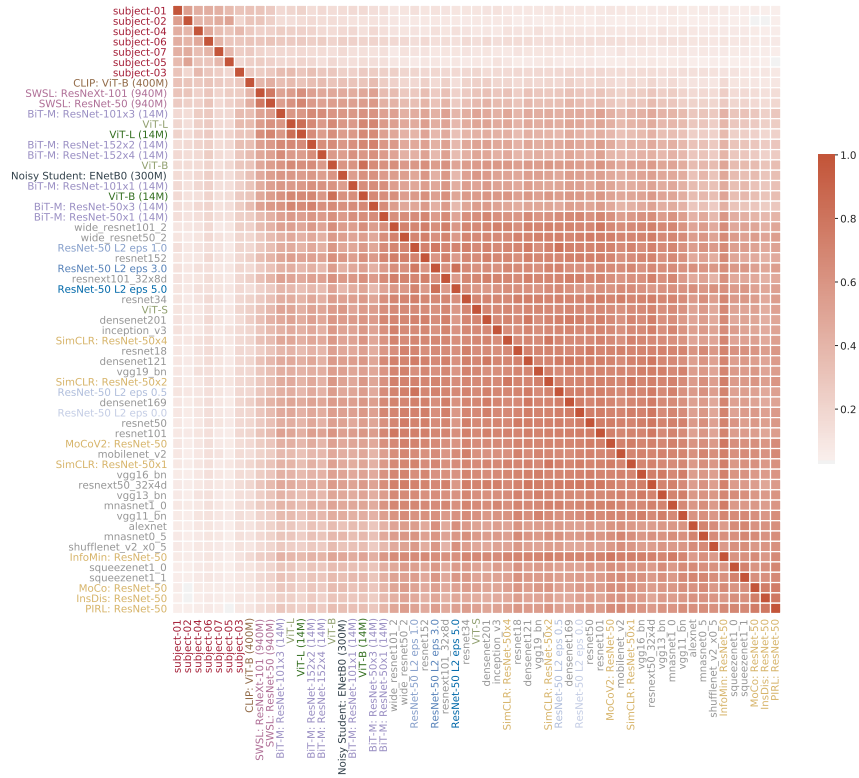


Figure 10: Error consistency for ‘sketch’ images (same as Figure 4 but sorted w.r.t. mean error consistency with humans).

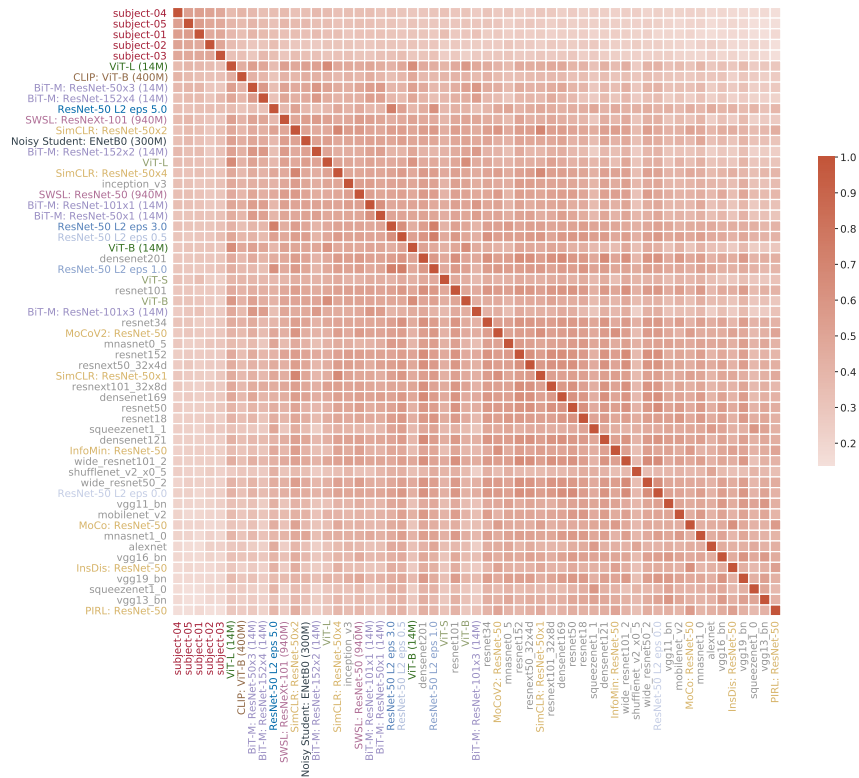


Figure 11: Error consistency for ‘stylized’ images (sorted w.r.t. mean error consistency with humans).



Figure 14: Error consistency for ‘cue conflict’ images (sorted w.r.t. mean error consistency with humans).

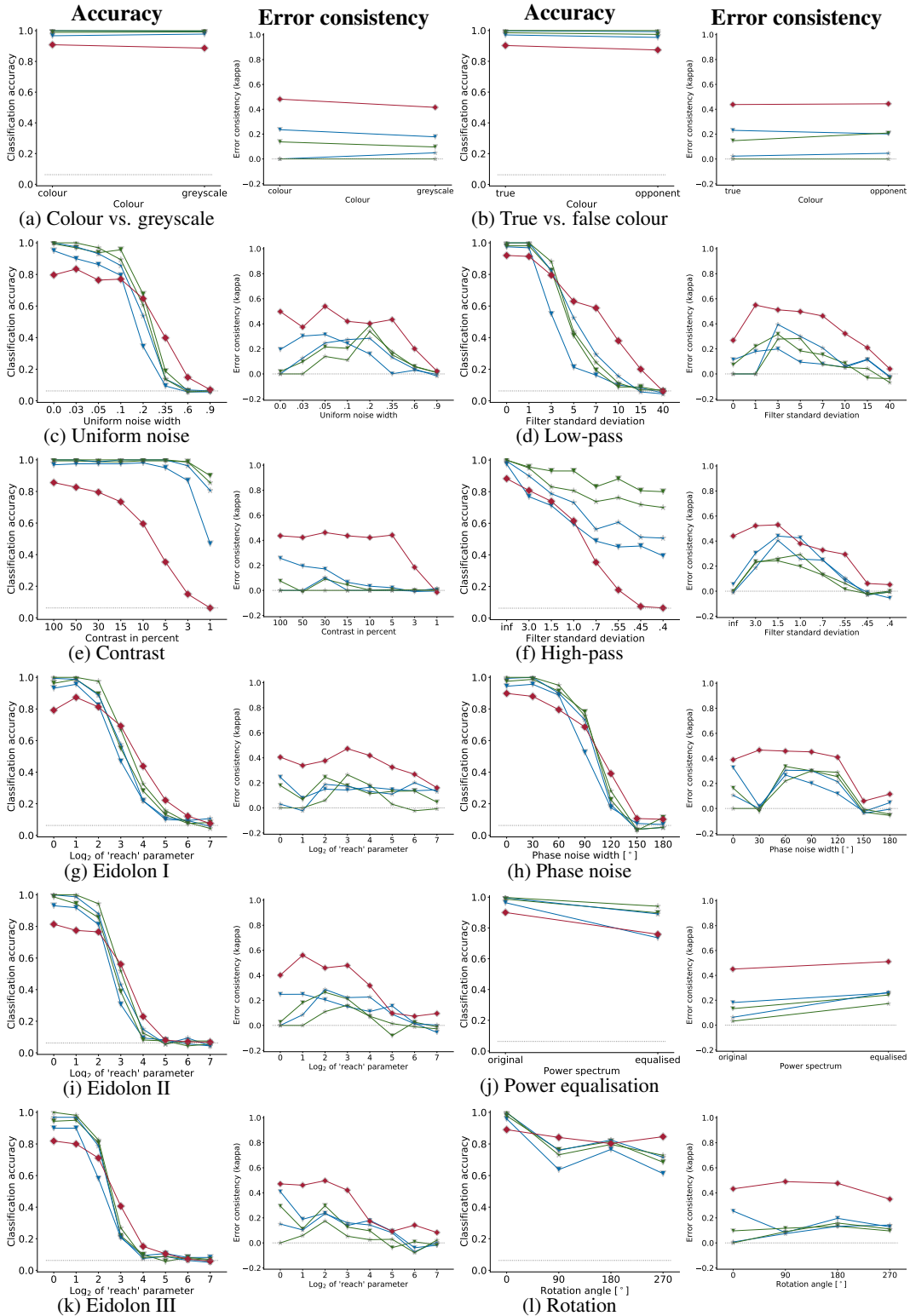


Figure 15: Comparison of self-supervised SimCLR models with supervised, augmentation-matched baseline models. Note that for better visibility, the colours and symbols deviate from previous plots. Plotting symbols: triangles for self-supervised models, stars for supervised baselines. Two different model-baseline pairs are plotted; they differ in the model width: blue models have 1x ResNet width [29], green models have 4x ResNet width [29]. For context, human observers are plotted as red diamonds. Baseline models kindly provided by Hermann et al. [47].

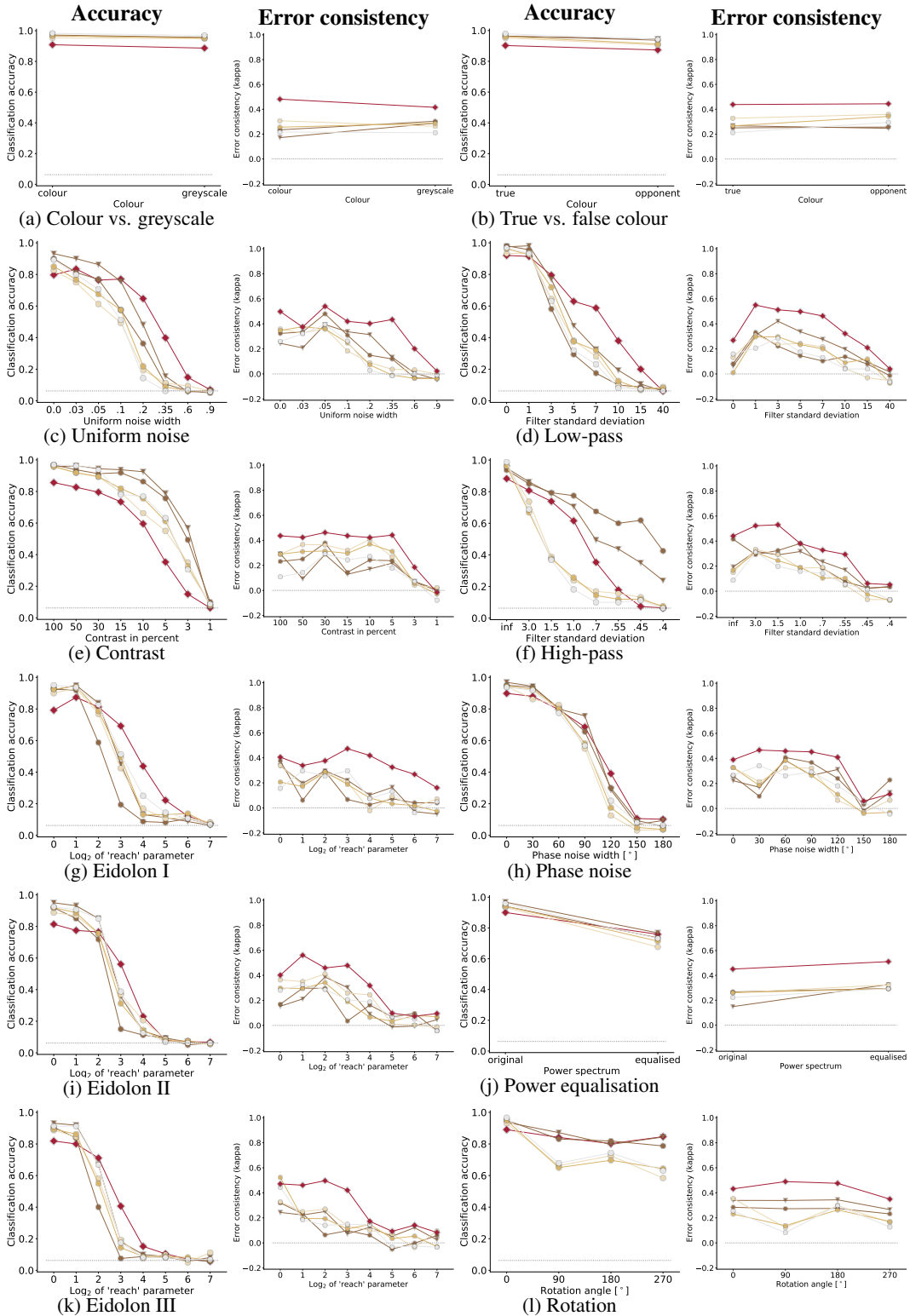


Figure 16: Do CLIP-provided labels lead to better performance? Comparison of standard ResNet-50 (light grey circles), CLIP with vision transformer backend (brown triangles), CLIP with ResNet-50 backend (brown circles), and standard ResNet-50 with hard labels (bright yellow circles) provided by evaluating standard CLIP on ImageNet; as well as human (red diamonds) for comparison. Symbols indicate architecture type (\circ convolutional, ∇ vision transformer, \diamond human); best viewed on screen. With the exception of high-pass filtered images, standard CLIP training with a ResNet-50 backbone performs fairly poorly.